



# Characterization of photovoltaic devices for indoor light harvesting and customization of flexible dye solar cells to deliver superior efficiency under artificial lighting



Francesca De Rossi<sup>a</sup>, Tadeo Pontecorvo<sup>b</sup>, Thomas M. Brown<sup>a,\*</sup>

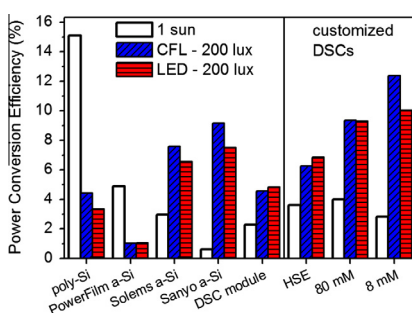
<sup>a</sup> CHOSE (Centre for Hybrid and Organic Solar Energy), Department of Electronic Engineering, University of Rome "Tor Vergata", via del Politecnico 1, 00133 Rome, Italy

<sup>b</sup> Department of Physics, University of Rome "La Sapienza", p.le Aldo Moro 2, 00185 Rome, Italy

## HIGHLIGHTS

- Experimental setup for photovoltaic measurements under indoor and low-level artificial light.
- Characterization of PV devices under commonly used illuminants (i.e. LED and CFL).
- Customization of flexible dye solar cells to deliver superior efficiency for light harvesting.
- Customized dye sensitized solar cells outperformed amorphous silicon devices at 200 lux.

## GRAPHICAL ABSTRACT



## ARTICLE INFO

### Article history:

Received 19 March 2015  
Received in revised form 8 June 2015  
Accepted 10 July 2015  
Available online 26 July 2015

### Keywords:

Energy harvesting  
Indoor measurements  
Amorphous silicon  
Polycrystalline silicon  
Dye sensitized solar cells  
Light harvesting

## ABSTRACT

The field of energy harvesting holds the promise of making our buildings “smart” if effective energy sources can be developed for use in ambient indoor conditions. Photovoltaics (PV), especially in its thin flexible form for easy integration, become a prime candidate for the aim, if tailored for low-density artificial light.

We designed a test system which enabled us to measure the performance of PV devices under compact fluorescent lamp (CFL) and light-emitting diode (LED) illumination at different illuminance levels and compared polycrystalline and amorphous silicon cells with our own flexible dye solar cells (DSCs). Whereas poly-Si cells, with 15% outdoor efficiency, delivered at 200 lux under CFL only  $2.8 \mu\text{W}/\text{cm}^2$  power density (and an efficiency of 4.4%), a-Si specifically designed for indoors, gave  $5.9 \mu\text{W}/\text{cm}^2$  and 9.2% efficiency under the same CFL conditions (and 7.5% efficiency under LED).

However, we show that the customization of flexible DSCs, by simply formulating ad-hoc less-concentrated, more transparent electrolytes, enabled these devices to outperform all others, providing average power densities of  $8.0 \mu\text{W}/\text{cm}^2$  and 12.4% efficiencies under 200 lux CFL (more than quadruple compared to those measured at 1 sun), and  $6.6 \mu\text{W}/\text{cm}^2$  and 10% efficiency under 200 lux LED illumination.

© 2015 Elsevier Ltd. All rights reserved.

## 1. Introduction

The development of a light harvesting technology that delivers remarkable output power in indoor and low-level light conditions

has tremendous potential for application in the field of domotics and building management systems [1–5]. It would enable the generation of a class of self-powered, easy-to-install devices, such as intelligent sensors that communicate wirelessly, cutting down maintenance costs and ensuring flexibility to building management systems without the need for changing pre-existing infrastructures, and thus helping the rapid growth of the potentially huge technology field of the “Internet of Things” [6].

\* Corresponding author.

E-mail address: [thomas.brown@uniroma2.it](mailto:thomas.brown@uniroma2.it) (T.M. Brown).

Solar cells are a prime candidate for harvesting available light inside buildings, even if they have been initially developed for and typically measured at Standard Test Conditions (STC), i.e. 1000 W/m<sup>2</sup> normal irradiation, with AM1.5G spectral coefficient and a temperature of 25 °C [7–11], which are fundamental in enabling comparison between panels and reliability and uniformity of testing worldwide but far from those usually experienced in indoor environments, both in the spectrum (which is mainly concentrated in the visible region whereas the sun has a strong component in the IR) and radiant light intensity (typically up to ~3 orders of magnitude smaller compared to those specified at STC).

During the last decade, a number of papers have monitored the performance of different photovoltaic technologies, such as crystalline silicon, amorphous silicon, DSCs, polymer PV and CIGS under full outdoor conditions [12–19]. Performance depends on the modules response to spectral, reflection, temperature, irradiance, and nominal power variations occurring throughout the day and the seasons [14]. It is thus important also to consider not only the total energy produced outdoors by different panels over the course of a time period [20,21] but also how the performance varies and responds to different parameters in varying operating conditions, including indoors.

Whereas crystalline silicon dominates the market for outdoor installations, with its spectral sensitivity designed to match natural sunlight, amorphous silicon (a-Si) and dye sensitized photovoltaic cells are the strongest candidates for indoor applications [5,22–25].

The technology of dye solar cells (DSCs) has attracted strong industrial interest [26,27] and even products have been launched. Flexible dye solar cells (DSCs) [25], in particular, being light weight and easy-to-tailor in shape and dimensions, represent not only a possible way to harvest more of the sunlight's energy over the device's footprint by increasing its capture area when used curved [21], but also an efficient and appealing technology for energy harvesting even from artificial light in buildings, delivering noteworthy power densities to feed a wide variety of sensors and devices [28]. Although the remarkable indoor performance of DSCs has been announced, especially by companies, such as Texas Instruments [24], Fujikura [29], G24 Power [30] and Ricoh [31], surprisingly – and presumably because of industrial secrecy and the lack of indoor measurement protocols – no studies on the customization of DSCs for indoor use are present in the literature.

Here, we first set up an indoor photovoltaic testing station which can be equipped with different artificial illumination sources and which allows photovoltaic measurement at different illuminance levels. We selected compact fluorescent lamps (CFLs) and light-emitting diodes (LEDs), being currently the most-used illuminants. Subsequently, we present a systematic study of different technologies for light harvesting, both rigid and flexible, monitoring their performance at different levels of illumination under both CFLs and LEDs, noting a very large variation when compared to measurements taken under a solar simulator at STC. The PV devices studied were poly-crystalline silicon (poly-Si), as the benchmark for outdoor PV, different forms (both flexible and rigid) of commercial a-Si, up till now the major technology used for integration in indoor applications (e.g. those found in light-powered calculators) and DSCs fabricated in our laboratories, in their thin flexible form that enables a potentially more seamless integration in electronic sensors and devices [25]. We show that whereas the efficiency of poly-Si drops very significantly when measured indoors, that of a number of a-Si and all DSCs (even those designed for STC) increases considerably. Finally, we customized flexible DSCs with a thin metal foil working electrode and a transparent plastic counterelectrode, formulating different electrolytes, not for STC, but to deliver impressive power densities under artificial

indoor lighting, demonstrating how their performance can be made to surpass that of even the best a-Si device we tested.

## 2. Materials and methods

### 2.1. PV cells and modules

Four types of solar cells based on different photovoltaic technologies, i.e. polycrystalline and amorphous silicon, were provided by the suppliers and/or manufacturers listed in Table 1 and compared in this study. The fifth type was a flexible parallel DSC module with the photoanode on titanium foil and an electrodeposited platinum counterelectrode, fabricated at our CHOSE labs according to a previously reported procedure that enables one to electrodeposit the Pt catalyst over large areas via conducting fingers, which then function also as the current collecting grid in completed modules [32]. The commercial electrolyte and dye used were HSE (Dyesol) and N719 (Dyesol) respectively.

### 2.2. Fabrication of small area DSCs and electrolyte formulation

Indium-doped tin oxide – coated polyethylene terephthalate, ITO/PET (Flexvue, 15 Ω/sq) was cut with a CO<sub>2</sub> laser in 2.5 × 2.5 cm<sup>2</sup> samples, which were ultrasonically cleaned in isopropyl alcohol for 10 min. Then the samples underwent platinum electrodeposition (with pulsed current method: 5 mA/cm<sup>2</sup>, 5 cycles,  $t_{on} = 1$  s,  $t_{off} = 4$  s) from an aqueous solution of 10 mM hexachloroplatinic acid, 10 mM potassium chloride and 10w% Triton X. A G300 potentiostat/galvanostat (Gamry Instruments Inc.) as the current source was used and a purpose-built three electrodes system, consisting of the ITO-PET sample as the working electrode, a Ti foil as the counterelectrode and an Ag/AgCl electrode as the reference electrode. After the electrodeposition, the platinized ITO-PET samples were rinsed with deionized water and dried at 100 °C for 15 min.

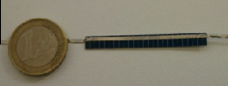


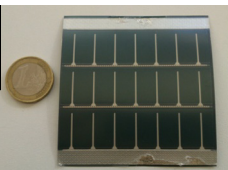
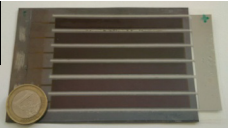
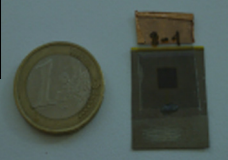
Electrolytes based on the iodide/triiodide ( $I^-/I_3^-$ ) redox couple in 3-methoxy-propionitrile (MPN) were prepared, changing the iodine concentration, i.e. 80, 40, 20 and 8 mM, while keeping constant the remaining components: 0.7 M tetrabutylammonium iodide (TBAI), as the iodide source, 0.15 M guanidinium thiocyanate, 0.15 M N-methylbenzimidazole. Please note that, as iodine associates readily with  $I^-$  to form  $I_3^-$ , the concentration of triiodide equals that of iodine, while the concentration of  $I^-$  is that of TBAI lowered by the concentration of iodine = triiodide, i.e. large excess. All the solvents and chemical reagents were purchased from Sigma Aldrich.

Titanium foil (125 μm, Goodfellow) was used as the photoanode substrate and polished both mechanically and chemically via H<sub>2</sub>O<sub>2</sub> immersion at 95 °C for 40 min, followed by a thermal annealing at 450 °C for 30 min. It was then immersed in a 40 mM aqueous solution of TiCl<sub>4</sub> solution at 70 °C for 30 min and rinsed in de-ionized water and in ethanol. An opaque TiO<sub>2</sub> paste (NR-AO Dyesol) was screenprinted on the Ti substrate and sintered at 525 °C for 30 min. TiCl<sub>4</sub> treatment was repeated and followed by a thermal process at 500 °C for 30 min. The final TiO<sub>2</sub> thickness was ~15 μm.

Photoanodes were sensitized by soaking into a 0.3 mM ruthenium-based N719 dye solution in ethanol overnight, washed with the same solvent and dried before cell assembly. Each photoelectrode was sealed together with a counterelectrode and the cell (0.5 × 0.5 cm<sup>2</sup> active area) was completed by injecting the  $I^-/I_3^-$ -based electrolytes with different iodine concentration. A commercial electrolyte, HSE from Dyesol, was also used for comparison.

**Table 1**

Details of the different PV devices employed in this study.

Technology	Model	Supplier/manufacturer	Active area (cm <sup>2</sup> )	Use	Image
Polycrystalline silicon (rigid)	Cell	Solar capture technologies	1.68	Outdoor	
Amorphous silicon (rigid)	05/048/016	Solems	6.63	Outdoor and indoor	
Amorphous silicon (rigid)	AM-1411	Sanyo	3.18	Indoor	
Amorphous silicon (flexible)	MPT3.6-75	Power Film	38.0	Outdoor	
Dye solar cell (flexible)	Parallel module	CHOSE	33.6	Outdoor	
Dye solar cell customized for indoor (flexible)	Test cell	CHOSE	0.25	Indoor	

### 2.3. Indoor photovoltaic measurement system

For characterization under typical artificial interior lighting, two different common light sources, namely a CFL (Lexman, class A, 39.2 lm/W electrical to optical efficacy) and LED (Lexman, class A+, 62.2 lm/W electrical to optical efficacy) were used. Irradiation from artificial light sources is generally expressed in photometric units (lux, illuminance) rather than radiometric ones (W/m<sup>2</sup>, irradiance), representing a measure of the light intensity as perceived by the human eye [22].

The spectral emission behavior of each lamp was recorded using a fiber optic spectrometer (BLACK-comet C-SR, Stellarnet Inc.) and Spectra Wiz software (that sets a  $\pm 5\%$  accuracy). Fig. 1 shows the measured emission spectra for both illuminants at 400 lux. By measuring the radiant flux and the luminous flux of each lamp, the luminous efficacy conversion factor (incident illuminance/incident irradiance) was calculated, being respectively  $(316 \pm 12)$  lm/W for CFL and  $(302 \pm 3)$  lm/W for LED. Those values were then used to evaluate the efficiency of the PV devices, since the respective inverse values multiplied by the measured illuminance level return the power density incident on the sample. The illuminance was appraised by a simple measure obtained using a luxmeter (Lafayette, model LM-1 with 0.1 lux resolution, overall accuracy of  $\pm 5\%$ , 4 digit readout).

Current–voltage (*I*–*V*) measurements under CFL and LED illumination were performed in a wooden box ( $0.4 \text{ m} \times 0.4 \text{ m} \times 0.7 \text{ m}$ ) with black walls and an E14 lamp holder incorporated at the top, as shown in Fig. 2. The incident power density was adjusted modifying the position along the *z* axis of the supporting plate, on which devices are placed for the measurement, in order to obtain the desired illuminance level on it. The opening was covered with

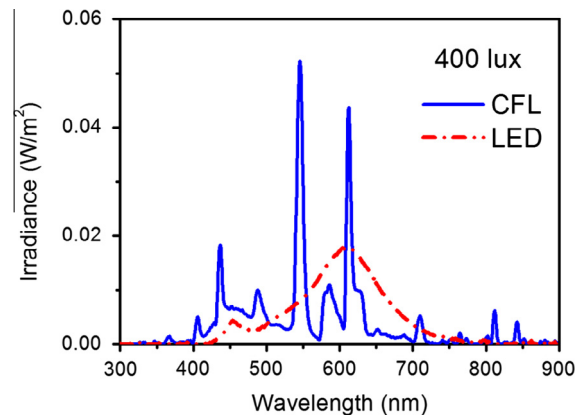


**Fig. 1.** Spectral irradiance measured at 400 lux for the artificial light sources used in this study, i.e. CFL and LED respectively.

a black curtain during *I*–*V* measurements to avoid ingress of light from the exterior.

The light bulbs employed in our system, namely CFL and LED, present irradiances which are orders of magnitude smaller than at STC and narrow emission spectra, with minor components in the IR range. Thus, the sources of heat which affect PV device efficiency [33] are minimized during indoor measurement. In fact, we observed that the temperature of the devices did not change from room temperature during all our measurements (21–22 °C).

The investigated lux levels ranged between 100 and 500 lux to cover a sufficient wide variety of indoor lighting conditions, with 100 lux typically found in the illumination of corridors [5],

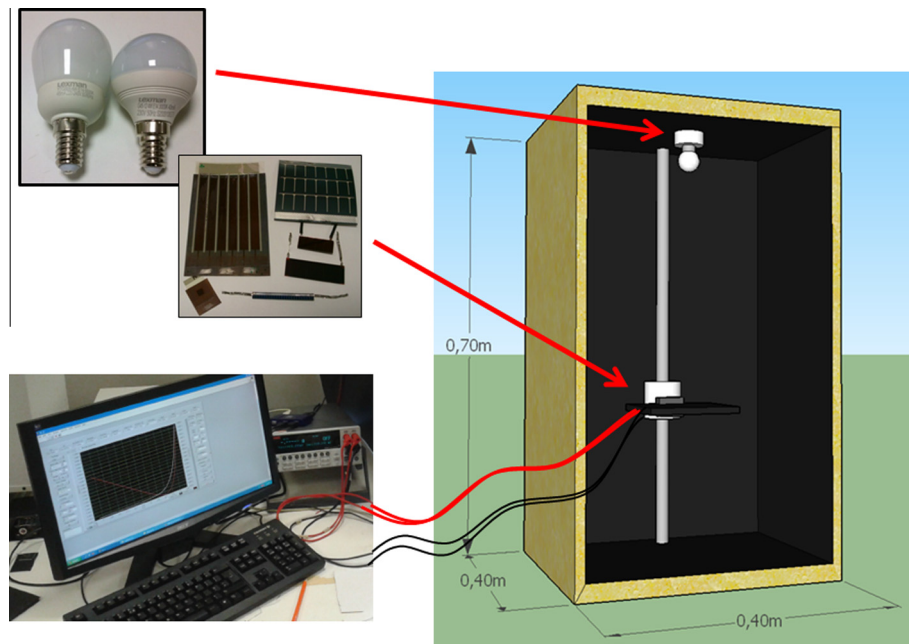


Fig. 2. Schematics of the setup for  $I$ - $V$  measurements under commonly used illuminants, i.e. CFL and LED.

200 lux in living rooms [34], and 300–500 lux in office environments [35]. It is worth mentioning that 1 sun radiation, i.e.  $1000 \text{ W/m}^2$  AM1.5G, corresponds to an illuminance of 100,000–110,000 lux [36,37].

Regarding the estimation of measurement errors, the contribution related to the electrical measurements with the Keithley Source measure unit is negligible ( $\ll 1\%$ ). The relative error of the incident optical power is  $\pm 10\%$  in relative terms, consisting of the sum of the accuracy of the illuminance measured by the luxmeter ( $\pm 5\%$ ) and the relative error of the luminous efficacy conversion factor ( $\pm 5\%$ ). Additionally, one has to consider the uniformity of the incident optical power over the plate area which we found to be negligible for the smaller devices (i.e. DSCs and a-Si Sanyo, since they are smaller than the luxmeter detector) and between 1% and 6% (increasing with illuminance level from 100 lux to 500 lux) for the larger devices (i.e. the DSC HSE module and a-Si PowerFilm). The uniformity of illumination is comparable to that specified for class B solar simulators [38]. Neglecting errors on the definition of device areas since these are large in this study [39], the maximum error (considering even the higher lux levels and device areas) on the PCE value is estimated to be  $\pm 16\%$  in relative terms.

Photovoltaic performance at 1 sun ( $1000 \text{ W m}^{-2}$ , AM 1.5) was measured with a computer-controlled Keithley 2420 source meter ( $\pm 0.012\%$  accuracy, 6 digits readout) under a sun simulator (SolarTest 1200 KHS Class B, equipped with a metal halogen bulb, 1200 W), using a Skye SKS 1110 sensor to set the incident power. The efficiencies under STC we measured for polycrystalline silicon cells were on average also within  $\pm 8\%$  in relative terms to the ones specified by the supplier. Furthermore, since it is well known that temperature is an important parameter to control during  $J$ - $V$  characterization and can affect the response of PV devices [33], an air cooling system was adopted to maintain the PV devices at  $25^\circ\text{C}$  during the current–voltage sweep.

#### 2.4. Absorption and external quantum efficiency measurements

Absorption spectra of N719 dye and iodine-based electrolyte solutions used for flexible DSCs were recorded using a spectrophotometer (Shimadzu UV–Vis 2550). The electrolyte solutions were

all diluted in MPN (ratio 1:600) to avoid the signal saturation of the spectrophotometer. Incident Photon-to-Current Conversion Efficiency (IPCE) measurements were carried out using a set-up consisting of a 150 W xenon lamp (Newport Model 70612) coupled with a monochromator (Cornerstone 130) and a Keithley 2420 source meter.

### 3. Results and discussion

#### 3.1. Comparison of PV technologies

It is well known that the output power of a solar cell depends on the spectral composition of the incident light, its intensity [32,40] and also the angle at which it is incident [41]. Therefore, a PV device should be optimized according to its final use or, vice versa, a proper utilization should be chosen for a PV device with a given spectral response. In Table 2, the photovoltaic parameters of the devices listed in Table 1 are reported, for different light sources and intensities.

The differences in  $V_{OC}$  in Table 2 are due to the fact that some devices are single cell while others are modules with series configuration. To simplify the comparison, we thus report and discuss hereafter only maximum power density ( $P_{MAX}$ ), power conversion efficiency (PCE), and short circuit current density ( $J_{SC}$ ), which all refer to unit area.  $J_{SC}$  values were obtained considering the active area of the unit cell, PCE and  $P_{MAX}$  values the active area of the entire device. Note that  $P_{MAX}$  is not perfectly equal to  $(J_{SC} \times FF \times V_{OC})/\text{number of cells}$ , due to small differences in device area and unit cell area.

Comparing the PCE of different devices under CFL and LED illuminance and under 1 sun irradiation, it is easy to infer or confirm the outdoor or indoor application each commercial device was designed or is best-suited for.

Poly-Si reduces its PCE from 15.1% in STC down to 6.1% ( $-60\%$ ) and even to 2.7% ( $-82\%$ ) under CFL, at 500 lux and 100 lux respectively. Flexible Power Film a-Si also suffers a drastic efficiency decrease, from 4.9% at STC to 1.8% and even 0.7% under CFL, at 500 lux and 100 lux respectively. This demonstrates they are intended for outdoor use.



**Table 2**  
Photovoltaic parameters for the commercial PV devices and the DSC module developed for STC (not customized for indoors, active area in brackets) under different light sources and illuminance levels.

Light source	Lux	Poly-Si Solar Capture Tech.						a-Si power film						a-Si Solems						a-Si Sanyo						DSC HSE module CHOSE							
		1 cell (1.68 cm <sup>2</sup> )						3 cells in series (38 cm <sup>2</sup> )						5 cells in series (6.63 cm <sup>2</sup> )						4 cells in series (3.18 cm <sup>2</sup> )						6 cells in parallel (33.6 cm <sup>2</sup> )							
		V <sub>oc</sub> V	J <sub>sc</sub> μA cm <sup>2</sup>	FF %	PCE %	P <sub>MAX</sub> μW cm <sup>2</sup>		V <sub>oc</sub> V	J <sub>sc</sub> μA cm <sup>2</sup>	FF %	PCE %	P <sub>MAX</sub> μW cm <sup>2</sup>		V <sub>oc</sub> V	J <sub>sc</sub> μA cm <sup>2</sup>	FF %	PCE %	P <sub>MAX</sub> μW cm <sup>2</sup>		V <sub>oc</sub> V	J <sub>sc</sub> μA cm <sup>2</sup>	FF %	PCE %	P <sub>MAX</sub> μW cm <sup>2</sup>		V <sub>oc</sub> V	J <sub>sc</sub> μA cm <sup>2</sup>	FF %	PCE %	P <sub>MAX</sub> μW cm <sup>2</sup>			
CFL	100	0.13	18.6	38.0	2.73	0.95	0.48	5.13	30.0	0.71	0.25	2.33	8.05	64.4	6.95	2.41	58.6	7.07	2.47	0.48	2.28	85.4	2.69	0.93									
	200	0.19	33.2	44.5	4.44	2.85	0.69	9.24	31.5	1.04	0.67	2.45	15.2	65.2	7.60	4.86	58.3	9.17	5.87	0.53	6.08	90.8	4.56	2.92									
	300	0.22	49.4	46.5	5.28	4.96	0.85	13.4	32.8	1.32	1.24	2.54	22.7	65.1	7.99	7.51	57.8	9.70	9.12	0.55	10.9	85.4	5.41	5.09									
	400	0.23	63.1	47.5	5.43	6.90	0.95	17.0	33.5	1.43	1.81	2.60	29.6	65.5	7.93	10.1	57.3	9.83	12.5	0.57	15.5	83.0	5.75	7.30									
	500	0.25	81.2	48.1	6.11	9.59	1.10	22.1	34.8	1.80	2.83	2.66	37.8	65.5	8.39	13.2	56.5	10.9	17.1	0.58	21.8	81.9	6.58	10.3									
LED	120	0.12	18.4	34.3	2.12	0.82	0.51	5.76	30.6	0.73	0.30	2.32	7.95	64.1	5.78	2.37	57.5	6.47	2.68	0.49	2.97	91.2	3.22	1.32									
	200	0.17	33.0	40.6	3.36	2.22	0.69	9.36	32.2	1.05	0.70	2.44	13.7	64.8	6.55	4.32	57.2	7.51	4.99	0.54	6.58	90.7	4.84	3.19									
	300	0.19	48.6	42.8	4.00	3.96	0.86	13.8	33.1	1.32	1.30	2.53	19.9	65.2	6.62	6.55	56.8	7.75	7.67	0.56	11.5	84.7	5.52	5.46									
	400	0.21	62.2	44.1	4.29	5.67	0.99	18.1	33.9	1.53	2.02	2.59	26.1	65.3	6.68	8.81	56.4	7.19	9.49	0.57	16.5	82.9	5.93	7.83									
	500	0.22	77.5	45.4	4.73	7.80	1.09	22.5	34.5	1.71	2.82	2.64	32.1	65.3	6.72	11.1	55.8	7.93	13.1	0.58	21.9	81.1	6.27	10.4									
1 sun	10 <sup>5</sup>	0.56	37.6·10 <sup>3</sup>	71.1	15.1	15.1·10 <sup>3</sup>	4.79	5.16·10 <sup>3</sup>	59.6	4.90	4.9·10 <sup>3</sup>	4.07	10.2·10 <sup>3</sup>	35.8	2.97	3.13·10 <sup>3</sup>	3.40	3.38·10 <sup>3</sup>	21.9	0.63	630	0.77	7.3·10 <sup>3</sup>	40.9	2.29	2.29·10 <sup>3</sup>							

On the contrary, Solems a-Si and Sanyo a-Si, as declared in their datasheets, are designed for indoors and, as a clear proof, their PCE improves tremendously, by 2–2.5 times and 10–15 times respectively, passing from simulated outdoor (i.e. STC) to artificial indoor light conditions. Both Solems a-Si and Sanyo a-Si deliver modest PCE at STC (3.0% and 0.6% respectively) but exhibit augmented efficiencies under CFL lighting, their PCE ranging from 7% at 100 lux up to 10% at 500 lux in the case of Sanyo a-Si.

Finally, the indoor PCE of the flexible DSC module, even though not designed for those conditions, also increases remarkably, from 2.3% at STC up to 6.6% at 500 lux CFL lighting, confirming the reported indoor light harvesting behavior of DSC technology [24,42]. Interestingly, it maintains the same and even delivers slightly higher efficiency when under LED rather than CFL light, whereas all the other technologies, except Power Film a-Si, suffer a 15–20% loss in efficiency at 200 lux and up to 27% at 500 lux when replacing CFL with LED illumination.

The reason for the observed behavior relates to the sensitivity of each technology to the spectral composition and the power density of the incident light [22,43]. Sunlight has a strong component in the IR range while CFL and LED lamps deliver much lower power densities and exhibit emission spectra mainly in the visible, as shown in Fig. 1.

Poly-Si is able to absorb light over a wide range of wavelengths, even in the IR region, and it delivered 15% power conversion efficiency under 1 sun normal irradiation, outperforming the other technologies. However, under low incident powers from narrower and low intensity CFL and LED illumination, its efficiency suffers [5,22,43], in our case by around a factor of 3.

DSC technology delivers better performance than poly-Si under interior lighting because it is able to sustain performance even at low incident power densities [32], and because of the good match between the emission spectra of the CFLs and LEDs with the absorption spectrum of the dye, as both of them mainly span the range of visible wavelengths only.

For all lux levels, regardless of the light source, Sanyo a-Si and Solems a-Si delivered the highest power densities – in the  $\mu\text{W}/\text{cm}^2$  range, but still enough, considering a small module of few cm<sup>2</sup> in area, for powering low power electronic devices, such as sensors, label, calculators, etc. For the a-Si devices there generally is a good spectral match between irradiance of the CFLs and LEDs and the IPCE curves (see Fig. 3).

Concerning a-Si based technologies, the observed different behavior between different models depends partly on their different spectral response, well-expressed by the IPCE curves of Fig. 3), related to differences in employed materials and fabrication processes [44]. Furthermore, it is likely that a-Si devices specifically targeted for indoor use have less conductive electrodes which are good for low level light (increasing transparency and/or the ratio between active area and total area) but not so at 1 sun since the FF drops very significantly at high power densities (see Table 2).

It is important to note that the DSC module, the PCE of which slightly exceeded the poly-Si cell, was fabricated using materials designed for operating under 1 sun solar illumination that is not optimized for indoor operation. In the next section, we will investigate an avenue for customization to increase, even more, the metal foil-based flexible DSC performance indoors.

### 3.2. Customization of the flexible DSC for indoor use via electrolyte iodine concentration

The flexible DSCs we manufactured, consist of a dye-sensitized titanium dioxide (TiO<sub>2</sub>) layer, screen-printed on an opaque thin titanium foil, a platinized counterelectrode on a transparent plastic substrate and an iodine-based electrolyte. In this architecture, the device is illuminated from its back (counterelectrode side) and the

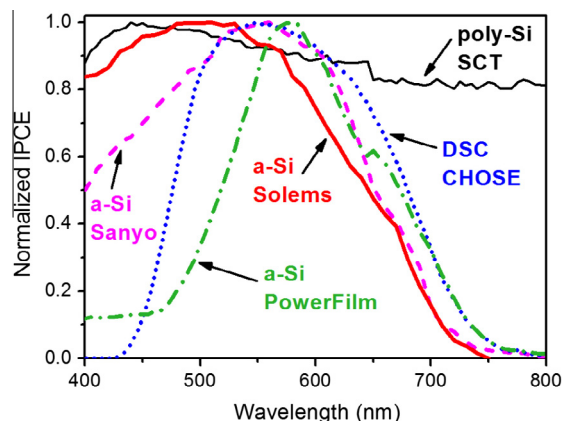


**Fig. 3.** Normalized incident photon-to-current efficiency (IPCE) spectra for the investigated PV devices across the visible range, i.e. where the CFL and LED emit light – see Fig. 1). Reported data for Solems a-Si and Sanyo a-Si were kindly provided by the respective manufacturers.

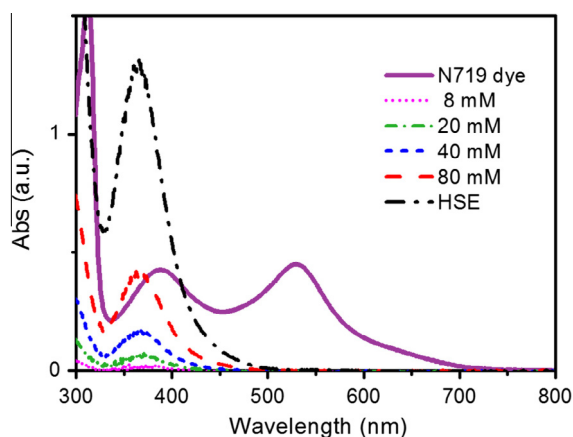


**Fig. 4.** Absorbance of N719 dye in ethanol (solid line) and of the electrolytes at different concentrations of iodine in MPN used in this study (HSE represents the commercial electrolyte).

incident light, before being absorbed by dye molecules, must pass throughout the electrolyte, absorbing a significant fraction of useful photons which are thus not able to reach the dye for wavelengths under 500 nm, as shown in Fig. 4.

Iodine concentration in the electrolyte affects both the effective cell operation and its transparency [45,46], the latter representing a crucial property for back-illuminated flexible DSCs [47]. We decided to modify the electrolyte by lowering the iodine ( $I_2$ ) concentration, which determines that of the triiodide ions ( $I_3^-$ ), since its strong absorption below 450–500 nm competes with the dye for light harvesting. As reported in Fig. 4, even our more concentrated electrolyte, i.e. 80 mM  $I_2$ , exhibited a considerable reduction in absorbance compared to that of the commercial HSE electrolyte, employed in the DSC module of Tables 1 and 2. We decreased the amount of iodine further, down to even a tenth (i.e. 8 mM), to investigate any improvements the enhanced transparency would bring to the PCE under indoor illumination and to lower electron recombination rates.

The conversion efficiency under 1 sun illumination of the cells with the different electrolyte remains constant for concentrations  $\geq 40$  mM, while it suffers for lower concentrations (see Fig. 5).

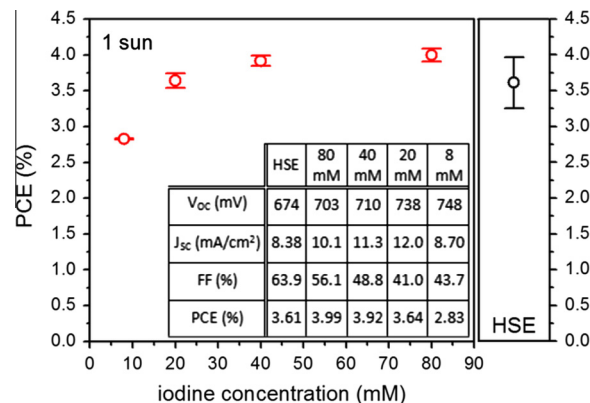


**Fig. 5.** Dependency of mean PCE on iodine concentration in the electrolyte for small, back illuminated flexible DSCs under 1 sun irradiation. A commercial electrolyte, HSE, was used as reference. Two cells for each electrolyte were fabricated and measured. The table in the inset reports mean PV parameters for the same cells.

This shows how common electrolytes are indeed tailored for STC operation, with the chosen  $[I_3^-]$  delivering good and stable operation at these conditions [45,46]. At STC, the consensus  $I_3^-$  concentrations ensure the rapid regeneration of the oxidized dye molecules after the photo-injection of electrons in the  $TiO_2$  ( $3I^- + 2D^+ \rightarrow 2D + I_3^-$ ) before relaxation of the excitation back to the ground state, also maintaining an excess reservoir of  $[I_3^-]$  for stable long term operation and a high diffusion-limited current [48,49]. Additionally,  $[I_3^-]$  is not too high as to excessively enhance the probability of recombination with free electrons at the photoanode before their collection.

A different behavior was observed for the same cells measured under various illuminance levels in our indoor setup endowed with either a CFL or a LED. An overall increase in PCE with decreasing iodine concentration was observed, at all illuminance levels and with both light sources. Interestingly, the highest PCE at these very low levels of light density was found for cells with the lowest 8 mM concentration. The same trend can be observed for  $J_{sc}$ , as shown in Fig. 6 for the case of 200 lux illuminance from the CFL source.

We focus our discussion on 200 lux illuminance since it represents both the typical lux level in most residential environments and a conservative choice, considering that illuminance in office environments ranges between 300 and 500 lux and, in this range, the PCE of our cells increases with incident light.

In these indoor conditions, the incident light is almost 3 orders of magnitude lower than that under a sun simulator. Thus, lowering of the  $[I_3^-]$ , even by over one order of magnitude compared to electrolytes developed for STC, has become possible, without photocurrents suffering from small diffusion limited currents or from high recombination rates because of a lack of dye-regenerating  $I_3^-$  ions, as they would have at higher light intensities, i.e. 1 sun. Actually, the flexible DSCs with the most transparent electrolyte, i.e. 8 mM, were able to convert up to 12.4% (mean value) of the incident optical power of the CFLs, with an overall enhancement of 244% and 97% compared to DSCs with HSE electrolyte tailored for outdoor use measured at STC (mean PCE = 3.61%) and under indoor CFL 200 lux lighting (mean PCE = 6.3%) respectively.

The almost linear  $J_{sc}$  increase was confirmed by IPCE measurements, performed using a xenon lamp emitting 350 lux at 550 nm (measured by spectrometer), thus comparable with incident light power coming from CFL and LED used in this study. IPCE spectra,

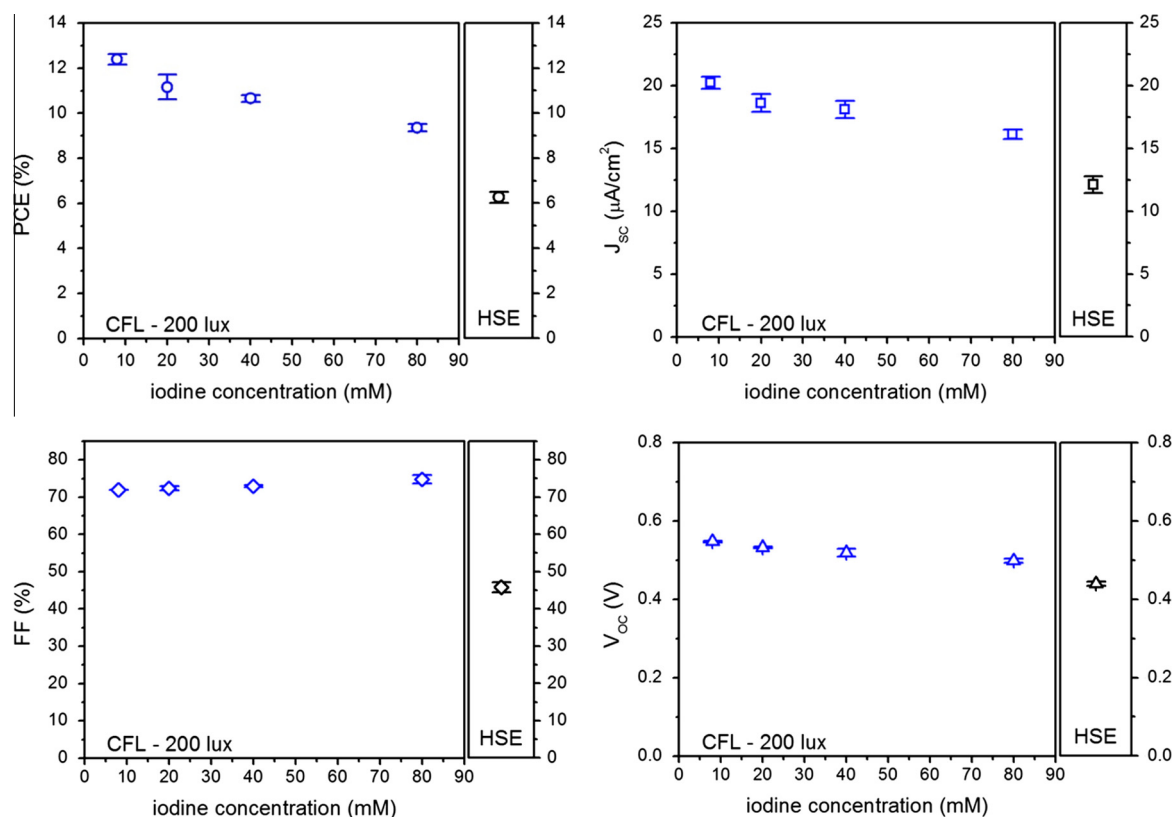


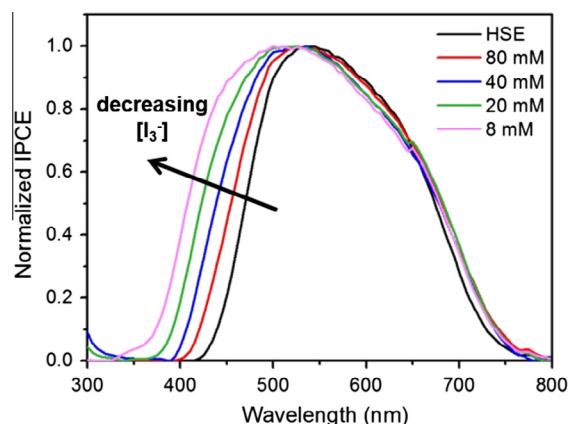
**Fig. 6.** Mean photovoltaic parameters under 200 lux CFL illumination for flexible back illuminated DSCs filled by electrolytes with different iodine concentration and commercial HSE for comparison. The best cell with 8 mM electrolyte under CFL at 200 lux gave PCE = 12.6%,  $V_{oc}$  = 549 mV,  $J_{sc}$  = 20.6  $\mu A/cm^2$ , FF = 71.9% and maximum power density equal to 8.10  $\mu W/cm^2$ .

reported in Fig. 7, revealed that, decreasing the iodine concentration, a larger fraction of incident photons were converted into electrons. This enhancement occurs mostly in the range where iodine strongly absorbs, i.e. below 450 nm (see Fig. 4): more photons are thus arriving to and being absorbed by the photoactive dye sensitized layer.

Comparing maximum power density values of these flexible DSCs different CFL lux levels (Fig. 8, left) to those measured for the PV devices of Tables 1 and 2 under the same lighting conditions, the flexible DSCs with the lowest iodine concentration in the electrolyte, namely 8 mM, outperformed (+19% at 200 lux, +11% at 500 lux) even the most efficient a-Si device, i.e. Sanyo. Even the maximum power density of the cell with the 80 mM  $[I_2]$  was very close to that of the best indoor a-Si cell, due to it being more transparent compared to commercial electrolytes developed for STC used in the DSC module. Under LED illumination, the effect is even more remarkable (Fig. 8, right): 8 mM iodine concentration leads to a 40% increase of maximum power density at 200 lux and up to 45% at 500 lux, compared to the most efficient a-Si under the same conditions.

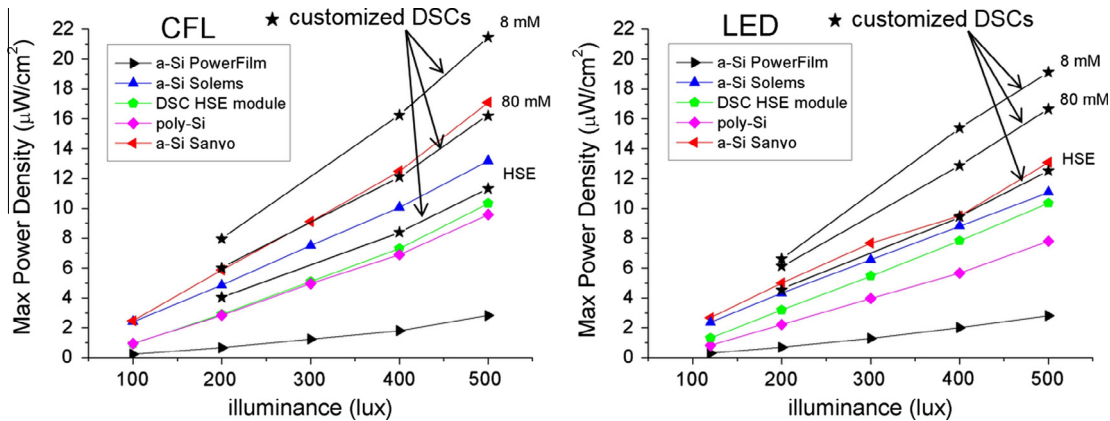
At 200 lux, in particular, the customized DSC with 8 mM electrolyte delivered 6.64 and 7.96  $\mu W/cm^2$  power density under respectively LED and CFL, i.e. an average of 7.3  $\mu W/cm^2$ . This value is very close to the 6.73  $\mu W/cm^2$  values specified by G24 Power at the same lux levels (although the lamp and PV device dimensions may be different) for flexible metal based DSCs [25,30].

Fig. 9 summarizes the PCE for all the PV devices of our study and the remarkable results achieved by the customization of DSCs, in the case of 200 lux illuminance from both CFL and LED sources: flexible customized DSCs were able to compete with and even outperform the most efficient a-Si devices.



**Fig. 7.** Normalized Incident photon-to-current efficiency (IPCE) spectra for flexible back illuminated DSCs incorporating electrolytes with different iodine concentrations. Also shown is the cell with the commercial HSE electrolyte for comparison.

Although this study was focused on the determination of the indoor PCE of PV technologies and the customization of DSCs for maximum efficiency under artificial lighting, we carried out a preliminary shelf life test. Fig. 10 shows the ratio between the efficiency after 7 months of the devices being left on a shelf and the initial value measured at 1 sun and at 200 lux under artificial lighting for the highest indoor-performing a-Si cell, the flexible a-Si cell, the DSC with the standard electrolyte and the DSC with 20 mM dilution.



**Fig. 8.** Maximum output power density at different light intensities for the investigated PV technologies under (left) CFL and (right) LED illumination, respectively, compared to the values obtained under the same conditions for small, back illuminated flexible DSCs (black stars) with different iodine concentrations. The cell with the lowest iodine concentration (8 mM) outperformed the most efficient a-Si device.

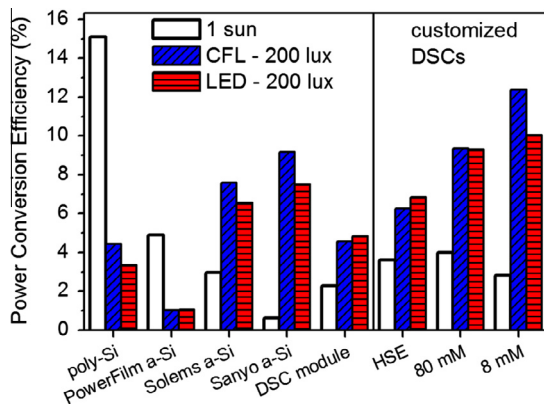


**Fig. 9.** Power conversion efficiency (PCE) of the investigated photovoltaic devices under CFL (blue bars with diagonal lines) and LED (red bars with horizontal lines) light sources at 200 lux illuminance, compared to values obtained under sun simulator at 1 sun illumination (white bars). The same data referring to small back-illuminated DSCs with the standard electrolyte, i.e. HSE, and customized electrolytes (80 and 8 mM iodine respectively) are also reported to highlight the gain achieved lowering the iodine concentration in the electrolyte itself. (For interpretation of the references to colour in this figure legend, the reader is referred to the web version of this article.)

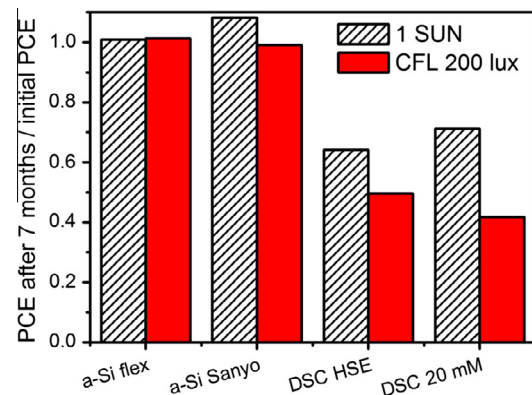


**Fig. 10.** Ratios between the PCE of a-Si and DSC devices after 7 months of shelf life at ambient conditions and the initial PCE value before the shelf life test. Ratios are reported for measurements at STC (1 sun) (dashed bars) and at 200 lux under CFL lighting (uniform red bars). (For interpretation of the references to colour in this figure legend, the reader is referred to the web version of this article.)

The a-Si devices showed good stability whilst the DSCs showed variation over time (in other studies we have noted some instances of even an increase in PCE presumably partially linked to electrolyte becoming more transparent over time due to bleaching). The first consideration is that commercial cells, based on mature technologies, are designed to fulfil high standard for quality and long-term use whereas laboratory cells are designed for more short-term measurement. Note that, since stability was not the objective of this particular study, we did not apply permeation barriers nor edge sealing to our DSCs, which would have significantly improved the long term performance of devices as we have demonstrated recently [50]. Furthermore, we noted that the commercial producer of flexible DSC technology G24 Power [30], specified 3 years of lifetimes in attuned indoor range (50–2000 lux and operating temperatures of 10–50 °C) for their product [25]. The second consideration is that indoor performance seems to age at a higher rate than that at STC over time.

These first results can help in the design of future systematic indoor stability studies, not only in determining protocols for indoor stability, which currently do not exist, but also to pinpoint,

with the help of characterization techniques, such as EIS, transient photovoltage decay, XRD etc., the more delicate material layers that give rise to differential ageing of devices when performance is measured under indoor and outdoor conditions.

Finally, it is interesting to mention what type of electronic devices the photovoltaic cells can power indoors assuming they are connected to an electronic regulator and to a storage/accumulator device so that the sensor (or other types of electronics) can function regularly (i.e. at determined time intervals). With the power densities delivered at 200 lux and 500 lux by our customized flexible DSCs, adapting the data from industrial laboratories, i.e. Fujikura [42], small sensors with operation cycle intervals of 10 s can be powered with accumulated energy from PV modules of respectively 41 and 15 cm<sup>2</sup> active area size. Increasing the area of the modules enables to power more energy-hungry devices (Table 3). The sizing depends strongly on efficiency of the PV module under the particular indoor ambient lighting that is present, the cycle time for sensing, the efficiency of the sensor and its wireless communication and also whether lighting is continually on or is intermittent. Thus, for energy harvesting it is important to develop power sources and accumulators and associated sensors/electronics which are as efficient as possible, the former in generating and storing power and the latter in using it. The incorporation of power



**Table 3**

Estimates for the size of PV devices (active area) necessary to deliver enough energy, accumulated over a 10 s cycle, to power different type of sensors at continuous 200 and 500 lux CFL or LED illumination. For the calculation, we used the maximum power densities (MPD) delivered by the customized dye solar cells (with 8 mM electrolyte) developed in this study and data from a Fujikura study [42] for the power consumption of the sensing/electronic devices, which usually depends greatly on design.

	Average illumination	200 lux LED	500 lux LED	200 lux CFL	500 lux CFL
	MPD of customized PV devices ( $\mu\text{W}/\text{cm}^2$ )	6.6	19.1	8.0	21.5
Electronic Devices	Energy Consumption (mW s) per Operation	Required active area ( $\text{cm} \times \text{cm}$ ) of the PV device for accumulating energy required over a 10 s cycle			
Low power sensors (e.g. temperature, gas, humidity)	3.3	$7.1 \times 7.1$	$4.2 \times 4.2$	$6.4 \times 6.4$	$3.9 \times 3.9$
Human movement sensors	7.5	$10.7 \times 10.7$	$6.3 \times 6.3$	$9.7 \times 9.7$	$5.9 \times 5.9$
Still cameras	13	$14 \times 14$	$8.3 \times 8.3$	$12.7 \times 12.7$	$7.8 \times 7.8$

functionalities into electronic objects can open up previously unavailable markets [51,52].

#### 4. Conclusions

We reported the output power densities and power conversion efficiencies (PCEs) of different PV technologies, both commercially available, namely polycrystalline and amorphous silicon, and developed in our laboratory, i.e. flexible DSC, under commonly used light sources for interior lighting, such as CFL and LED.

We focused on 200 lux illuminance being the typical lux level in most residential environments and at the same time representing a conservative choice, since illuminance in office environments ranges between 300 and 500 lux and PCE in this range increases with incident light.

We found that the PCE of PV technologies intended for outdoors reduces drastically when operating under indoor lighting, e.g. from 15.1% in STC down to 4.44% and 3.36% under 200 lux from CFL and LED respectively in the case of poly-Si. Results show that even a-Si devices need to be specifically tailored for indoors to deliver high efficiencies in these conditions: a-Si devices optimized for indoors, despite their modest PCE at STC (2.97% for Solems a-Si and 0.63% for Sanyo a-Si), exhibit augmented efficiencies under CFL lighting, their PCE ranging from 7.6% (Solems) to 9.2% (Sanyo) at 200 lux. Similar but smaller gains were achieved when replacing CFL with LED illumination (6.5% for Solems, 7.5% for Sanyo).

The PCE of the flexible DSC module fabricated in our labs, even though intended for outdoor operation, increased from 2.3% at STC to 4.6% at 200 lux under CFL lighting, delivering even slightly higher efficiencies under LED.

Finally, we demonstrated the need for tailoring the DSC components, first of all the electrolyte, especially for back-illuminated devices, according to the intended operating conditions, i.e. indoors in this study. In particular, decreasing the iodine concentration in the electrolyte, the main responsible for optical losses, we observed considerable improvement in photogenerated currents mainly due to higher transparency of the electrolyte, without losing in dye regeneration efficiency since the incident light is up to 3 orders of magnitude lower than under full simulated sunlight.

Flexible DSCs with the lowest iodine concentration in the electrolyte (8 mM) reached at 200 lux under CFL illumination the mean efficiency value of 12.4%, more than 4 times higher than mean PCE at STC, i.e. 2.8%, and delivered maximum power density of  $8 \mu\text{W}/\text{cm}^2$  at 200 lux, (and  $21.5 \mu\text{W}/\text{cm}^2$  at 500 lux), 35% higher than that obtained for the most efficient a-Si device measured in this study in the same conditions.

These remarkable enhancements demonstrate the outstanding capabilities of flexible DSCs under indoor lighting, obtained by acting on the electrolyte only. Further optimization may be directed towards  $\text{TiO}_2$ , compact layer and dye optimization for attaining further gains in the future together with systematic stability tests designed for the indoors.

#### Acknowledgments

Authors would like to thank Prof. M. Capizzi (University of Rome – La Sapienza) for useful discussions and his excellent lecture course on device physics and F. Di Giacomo (University of Rome – Tor Vergata) for advice about electrolyte formulation; Dr. A. Labouret (Solems S.A.) for providing a-Si devices and the relative IPCE data, Dr. S. Dunnill (Solar Capture Technologies Ltd.) for providing crystalline Si cells, Dr. S. Ishihara (Panasonic Electric Works Europe AG) for providing the IPCE spectrum of Sony a-Si device. We thank “Polo Solare Organico” Regione Lazio, the FP7 project CHEETAH n. 609788, and the “AQUASOL” PRIN 2012 (2012A4Z2RY) projects for funding.

#### References

- [1] Matiko J, Grabham N, Beeby S, Tudor M. Review of the application of energy harvesting in buildings. *Meas Sci Technol* 2014;25:012002.
- [2] Gorlatova M, Kinget P, Kymissis I, Rubenstein D, Wang X, Zussman G. Energy harvesting active networked tags (EnHANTs) for ubiquitous object networking. *Wireless Commun IEEE* 2010;17:18–25.
- [3] Collado A, Georgiadis A. Conformal hybrid solar and electromagnetic (EM) energy harvesting rectenna. *IEEE Trans Circ Syst I – Regular Papers* 2013;60:2225–34.
- [4] Niotaki K, Collado A, Georgiadis A, Sangkil K, Tentzeris MM. Solar/electromagnetic energy harvesting and wireless power transmission. *Proc IEEE* 2014;102:1712–22.
- [5] Reich N, Van Sark W, Turkenburg W. Charge yield potential of indoor-operated solar cells incorporated into Product Integrated Photovoltaic (PIPV). *Renewable Energy* 2011;36:642–7.
- [6] Jayakumar H, Lee K, Lee WS, Raha A, Kim Y, Raghunathan V. Powering the internet of things. In: *Proceedings of the 2014 international symposium on low power electronics and design*; ACM; 2014. p. 375–80.
- [7] Hardin BE, Snaith HJ, McGehee MD. The renaissance of dye-sensitized solar cells. *Nat Photonics* 2012;6:162–9.
- [8] Kroon J, Bakker N, Smit H, Liska P, Thampi K, Wang P, et al. Nanocrystalline dye-sensitized solar cells having maximum performance. *Prog Photovoltaics Res Appl* 2007;15:1–18.
- [9] Shrotriya V, Li G, Yao Y, Moriarty T, Emery K, Yang Y. Accurate measurement and characterization of organic solar cells. *Adv Funct Mater* 2006;16:2016–23.
- [10] Green MA. The path to 25% silicon solar cell efficiency: history of silicon cell evolution. *Prog Photovoltaics Res Appl* 2009;17:183–9.
- [11] Green MA, Emery K, Hishikawa Y, Warta W, Dunlop ED. Solar cell efficiency tables (version 43). *Prog Photovoltaics Res Appl* 2014;22:1–9.
- [12] Gottschalg R, Del Cueto JA, Betts TR, Infield DG. Seasonal performance of a-Si single- and multijunction modules in two locations. *Photovoltaic Specialists. Thirty-first IEEE*; 2005.
- [13] Jardine CN, Conibeer GJ, Lane K. PV-COMPARE: direct comparison of eleven PV technologies at two locations in northern and southern Europe. *Seventeenth EU PVSEC*. Munich; 2001.
- [14] Pierro M, Bucci F, Cornaro C. Full characterization of photovoltaic modules in real operating conditions: theoretical model, measurement method and results. *Prog Photovoltaics Res Appl* 2015;23:443–61.
- [15] Cornaro C, Bartocci S, Musella D, Strati C, Lanuti A, Mastroianni S, et al. Comparative analysis of the outdoor performance of a dye solar cell mini-panel for building integrated photovoltaics applications. *Prog Photovoltaics Res Appl* 2015;23:215–25.
- [16] Radue C, van Dyk EE, Macabebe EQ. Analysis of performance and device parameters of CIGS PV modules deployed outdoors. *Thin Solid Films* 2009;517:2383–5.
- [17] Hauch JA, Schilinsky P, Choulis SA, Childers R, Biele M, Brabec CJ. Flexible organic P3HT:PCBM bulk-heterojunction modules with more than 1 year outdoor lifetime. *Sol Energy Mater Sol Cells* 2008;92:727–31.

- [18] del Cueto JA, Rummel S, Kroposki B, Osterwald C, Anderberg A. Stability of CIS/CIGS modules at the outdoor test facility over two decades. *Photovoltaic Specialists Conference, 2008 PVSC '08 33rd IEEE*; 2008. p. 1–6.
- [19] Ishii T, Takashima T, Otani K. Long-term performance degradation of various kinds of photovoltaic modules under moderate climatic conditions. *Prog Photovoltaics Res Appl* 2011;19:170–9.
- [20] Reale A, Cinà L, Malatesta A, De Marco R, Brown TM, Di Carlo A. Estimation of energy production of dye-sensitized solar cell modules for building-integrated photovoltaic applications. *Energy Technol* 2014;2:531–41.
- [21] Zardetto V, Mincuzzi G, De Rossi F, Di Giacomo F, Reale A, Di Carlo A, et al. Outdoor and diurnal performance of large conformal flexible metal/plastic dye solar cells. *Appl Energy* 2014;113:1155–61.
- [22] Li Y, Grabham NJ, Beeby SP, Tudor M. The effect of the type of illumination on the energy harvesting performance of solar cells. *Sol Energy* 2015;111:21–9.
- [23] Sacco A, Rolle L, Scaltrito L, Tresso E, Pirri CF. Characterization of photovoltaic modules for low-power indoor application. *Appl Energy* 2013;102:1295–302.
- [24] Sridhar N, Freeman D. A Study of dye sensitized solar cells under indoor and low level outdoor lighting: comparison to organic and inorganic thin film solar cells and methods to address maximum power point tracking. In: 26th European photovoltaic solar energy conference and exhibition; 2011. p. 232–6.
- [25] Brown T, De Rossi F, Di Giacomo F, Mincuzzi G, Zardetto V, Reale A, et al. Progress in flexible dye solar cell materials, processes and devices. *J. Mater. Chem. A* 2014;2:10788–817.
- [26] Hinsch A, Veurman W, Brandt H, Flarup Jensen K, Mastroianni S. Status of dye solar cell technology as a guideline for further research. *ChemPhysChem* 2014;15:1076–87.
- [27] Fakharuddin A, Jose R, Brown TM, Fabregat-Santiago F, Bisquert J. A perspective on the production of dye-sensitized solar modules. *Energy Environ Sci* 2014;7:3952–81.
- [28] Reich N, Veefkind M, Sark Wv, Alsema E, Turkenburg W, Silvester S. A solar powered wireless computer mouse: industrial design concepts. *Sol Energy* 2009;83:202–10.
- [29] Fujikura. Fujikura dye-sensitized solar cells now offer 18% energy conversion efficiency, <[http://www.fujikura.co.jp/eng/f-news/2035577\\_4207.html](http://www.fujikura.co.jp/eng/f-news/2035577_4207.html)>; 2012.
- [30] G24 Power Ltd. <http://gcell.com/>.
- [31] Ricoh L. Complete solid-state dye-sensitized solar cell. <[http://www.ricoh.com/about/company/technology/tech/066\\_dssc.html](http://www.ricoh.com/about/company/technology/tech/066_dssc.html)>; 2014.
- [32] De Rossi F, Brown TM, Reale A, Di Carlo A. Large-area electrodeposition of counterelectrodes utilizing the same integrated conductive grid for fabrication of parallel flexible dye solar cell modules. *IEEE J Photovolt* 2014;4:1552–9.
- [33] Raga SR, Fabregat-Santiago F. Temperature effects in dye-sensitized solar cells. *Phys Chem Chem Phys* 2013;15:2328–36.
- [34] Sridhar N, Freeman D. Bringing PV indoors again, <[http://www.electronicproducts.com/Power\\_Products/Invertors/Bringing\\_PV\\_indoors\\_again.aspx](http://www.electronicproducts.com/Power_Products/Invertors/Bringing_PV_indoors_again.aspx)>; 2011.
- [35] Richman EE. Requirements for lighting levels. <[https://www.wbdg.org/pdfs/usace\\_lightinglevels.pdf](https://www.wbdg.org/pdfs/usace_lightinglevels.pdf)>; 2012.
- [36] Kandilli C, Ulgen K. Solar illumination and estimating daylight availability of global solar irradiance. *Energy Sources Part A* 2008;30:1127–40.
- [37] Castaner L, Silvestre S. Modelling photovoltaic systems using PSpice. John Wiley and Sons; 2002.
- [38] Emery K. Solar simulators and I–V measurement methods. *Sol Cells* 1986;18:251–60.
- [39] Ito S, Nazeeruddin M, Liska P, Comte P, Charvet R, Péchy P, et al. Photovoltaic characterization of dye-sensitized solar cells: effect of device masking on conversion efficiency. *Prog Photovoltaics Res Appl* 2006;14:589–601.
- [40] Reich N, Van Sark W, Alsema E, Lof R, Schropp R, Sinke W, et al. Crystalline silicon cell performance at low light intensities. *Sol Energy Mater Sol Cells* 2009;93:1471–81.
- [41] D'Ercole D, Dominici L, Brown TM, Michelotti F, Reale A, Di Carlo A. Angular response of dye solar cells to solar and spectrally resolved light. *Appl Phys Lett* 2011;99:213301.
- [42] Tanabe N. Dye-sensitized solar cell for energy harvesting applications. Fujikura Technical Review; 2013.
- [43] Randall J, Jacot J. The performance and modelling of 8 photovoltaic materials under variable light intensity and spectra. World Renewable Energy Congress VII & Expo (No LPM-CONF-2002-006); 2002.
- [44] Rütther R, Kleiss G, Reiche K. Spectral effects on amorphous silicon solar module fill factors. *Sol Energy Mater Sol Cells* 2002;71:375–85.
- [45] Hao F, Lin H, Zhang J, Zhuang D, Liu Y, Li J. Influence of iodine concentration on the photoelectrochemical performance of dye-sensitized solar cells containing non-volatile electrolyte. *Electrochim Acta* 2010;55:7225–9.
- [46] Yu Z, Gorlov M, Nissfolk J, Boschloo G, Kloo L. Investigation of iodine concentration effects in electrolytes for dye-sensitized solar cells. *J Phys Chem C* 2010;114:10612–20.
- [47] De Rossi F, Di Gaspare L, Reale A, Di Carlo A, Brown TM. Blending CoS and Pt for amelioration of electrodeposited transparent counterelectrodes and the efficiency of back-illuminated dye solar cells. *J Mater Chem A* 2013;1:12941–7.
- [48] Mastroianni S, Lembo A, Brown TM, Reale A, Di Carlo A. Electrochemistry in reverse biased dye solar cells and dye/electrolyte degradation mechanisms. *ChemPhysChem* 2012;13:2964–75.
- [49] Mastroianni S, Asghar I, Miettunen K, Halme J, Lanuti A, Brown TM, et al. Effect of electrolyte bleaching on the stability and performance of dye solar cells. *Phys Chem Chem Phys* 2014;16:6092–100.
- [50] De Rossi F, Mincuzzi G, Di Giacomo F, Fahlteich J, Amberg-Schwab S, Noller K, et al. Improved stability of flexible dye solar cells via application of ultra high permeation barriers. Submitted for publication.
- [51] Rosa P, Câmara A, Gouveia C. The potential of printed electronics and personal fabrication in driving the internet of things. *Open J Internet Things* 2015;1:16–36.
- [52] Want R, Schilit BN, Jenson S. Enabling the Internet of Things. *Computer* 2015;48:8–35.